Origin of Northeast Fujian Basalts and Limitations on the Heterogeneity of Mantle Sources for Cenozoic Alkaline Magmatism across SE China: Evidence from Zircon U-Pb Dating, Petrological, Whole-Rock Geochemical, and Isotopic Studies

Guishan Zhang [1,2,3,*], **Ren Peng** [1,*], **Hongxin Qiu** [1], **Hanjie Wen** [3], **Yonggang Feng** [1], **Baoyun Chen** [1], **Lei Zhang** [1], **Shen Liu** [4] **and Taotao Liu** [1]

[1] School of Earth Science and Resources, Chang'an University, Xi'an 710065, China; hxqiu1@126.com (H.Q.); ygfeng@chd.edu.cn (Y.F.); baoyun1114@chd.edu.cn (B.C.); zhanglei211@chd.edu.cn (L.Z.); liutaotao188@163.com (T.L.)

[2] Key Laboratory of Western China Mineral Resources and Geological Engineering, Ministry of Education, Xi'an 710065, China

[3] Institute of Geochemistry, Chinese Academy of Sciences, Guiyang 550081, China; wenhanjie@vip.gyig.ac.cn

[4] State Key Laboratory of Continental Dynamics and Department of Geology, Northwest University, Xi'an 710069, China; liushen@vip.gyig.ac.cn

* Correspondence: zygszh@chd.edu.cn (G.Z.); pengren21@126.com (R.P.)

Abstract: Cenozoic alkali basalts in Southeast (SE) China generally are genetically related to intracontinental rifting. Hence, they can be used to probe the nature of their underlying mantle sources and aid studies of the tectonic background in this region. This paper focuses on the Shanhoujian alkali basalts located in Bailing County, northeastern Fujian, SE China. We herein report their petrology, whole-rock major, and trace element geochemistry, and Sr-Nd isotopic composition and provide a new zircon U-Pb age for the basalts (~40 Ma, Eocene). These data help to constrain the petrogenesis of alkali basalts, their mantle source, and tectonic settings. The basalts are characterized by high Mg$^{\#}$ (58.21–63.52) with $Na_2O/K_2O > 1$. MgO content is weakly correlated with CaO and Cr content but shows no correlation with Ni and Fe_2O_3 (total). Such features suggest that fractionation of clinopyroxene rather than olivine was important. In terms of trace elements, the alkali basalts display: (1) enrichment in La, Ce, Rb, Ba, Nb, and Ta and depletion in K, Pb, Zr, Hf, and Ti and (2) notable fractionation of light rare earth elements from heavy rare earth elements. Determined $(^{87}Sr/^{86}Sr)_i$ is in the range of 0.7041–0.7040 and ε_{Nd} (t) is between +3.2 and +3.3. The Shanhoujian alkali basalts show a notable affinity to oceanic island basalts (OIBs) with little assimilation of crustal materials. They were derived from a pyroxenite and carbonated peridotite mantle source metasomatized by sediments carried by the subduction plate at different depths. The primary magmas of these basalts were derived from partial melting of this metasomatized mantle source during upwelling of the asthenospheric mantle as an intracontinental rift formed through extension in this part of SE China.

Keywords: alkali basalts; pyroxenes; carbonated peridotite; continental rift; NE Fujian

1. Introduction

Alkali basalts are predominantly distributed within intraoceanic and intracontinental plates. There are two main opinions about the formation of oceanic alkali basalts: (1) they were formed from recycled materials of subducted oceanic crust [1,2] and (2) they were derived from partial melting of the

metasomatized mantle source [3–5]. There are several arguments regarding the formation and genesis of continental alkali basalts, such as that they were derived from an asthenosphere mantle source [6], a mixture of asthenospheric and lithospheric materials [7], or source mantle containing recycled crustal materials [8,9]. Experimental results demonstrated that the mantle source for alkali basalts contained significant pyroxenites, hornblendites, and carbonated peridotites [4,10–14]. Mantle pyroxenite is closely related to subduction and associated collision, and is commonly metasomatized in the channel of subduction and collision [15,16]. Therefore, it is important to investigate the components of the mantle source of alkali basalts.

Alkali basalts in the coastal areas of Southeast (SE) China are important components of the Circum-Pacific volcanic belts, drawing much attention by geologists around the world. Although those alkali basalts have been extensively dated, their genesis and mantle sources are still open to debate [6,17–21]. Previous studies on alkali basalts mainly focused on the Longhai–Mingxi district [6,17], Fujian Province, which contains the predominant volume of alkali basalts in the coastal areas of SE China. By contrast, alkali basalts in other areas of Fujian Province have not been fully studied [22]. This paper focuses on the Shanhoujian alkali basalts in the northeastern part of the province and explores their petrogenesis using petrological and geochemical methods. Further, this paper discusses the mantle source and tectonic setting in light of trace elements and isotopic compositions in combination with the Cenozoic tectonic evolution of SE China.

2. Geological Background and Petrology

SE China is tectonically ascribed to the South China Block, which is bounded by the Qinling–Dabie orogenic belt to the north, adjacent to the Tibet Plateau in the west, and linked to the Western Pacific tectonic domain (Figure 1). The South China Block is supposed to have formed through a collision between the Yangtze and Cathaysia blocks in the late Proterozoic [23]. The Yangtze and Cathaysia blocks are bounded by the Jiangshan–Shaoxing–Pingxiang fault with different basement materials and crust–mantle structure [24]. Large-scale Mesozoic and Cenozoic volcanic-intrusive complex belts are exposed in SE China. Cenozoic magmatism mainly produces mafic volcanic rocks, e.g., basalts, whose distribution is controlled by Zhenghe–Dapu and Changle–Nan'ao faults with NE strikes (Figure 1b). Cenozoic basalts in the coastal area of SE China are exposed along a NE orientation from the coast to inland. The Cenozoic basalts mainly include alkaline, alkaline olivine, and tholeiitic basalts [17]. Mantle xenoliths, which are contained in alkaline basalts, are dominated by spinel lherzolite, spinel harzburgite, and garnet lherzolite [25]. In terms of formation age, the Cenozoic basalts in Fujian show a trend of gradually getting younger from the coast to inland. The formation ages of basalts from Longhai and Fuding on the east coast are 17.1–14.9 Ma and 40.1 Ma (as shown in this paper), respectively. The age of Miqing basalts in central Fujian is 11.9 Ma and of Mingxi basalts in western Fujian is 1.2–2.3 Ma [17].

The study area is located at Bailin town, Fuding city, northeastern Fujian Province, and is situated on the southeastern margin of the Eurasia plate, which is part of the Circum-Pacific Mesozoic and Cenozoic huge magmatic belts (Figure 1). The Shanhoujian alkali basalts overlie the lower Cretaceous Shimaoshan pyroclastic rocks, exhibiting a volcanic pipe with the shape of an inverted cone in cross-section. The volcanic pipe has an opposite dip, and the dip angle gradually increases from top to bottom. These rocks have an irregular elliptical morphology with a NW-striking long axis in the plane, and form roughly circular zonation from explosive volcanic breccias in the inner portion to flood basalts and subvolcanic olivine gabbro–basalts [22], indicating a central eruption style. Explosive volcanic breccias that are exposed in the west and north of the basalt pipe consist of rounded deep mantle xenoliths and subangular wall-rock, crystal, and cement minerals. Flood basalts are also exposed in the west and north of the basalt pipe, inside volcanic breccias, and contain a small amount of mantle peridotite xenoliths. The main body of the volcanic pipe is composed of subvolcanic olivine gabbro–basalt with the typical hexagonal columnar jointing (Figure 2a) [22].
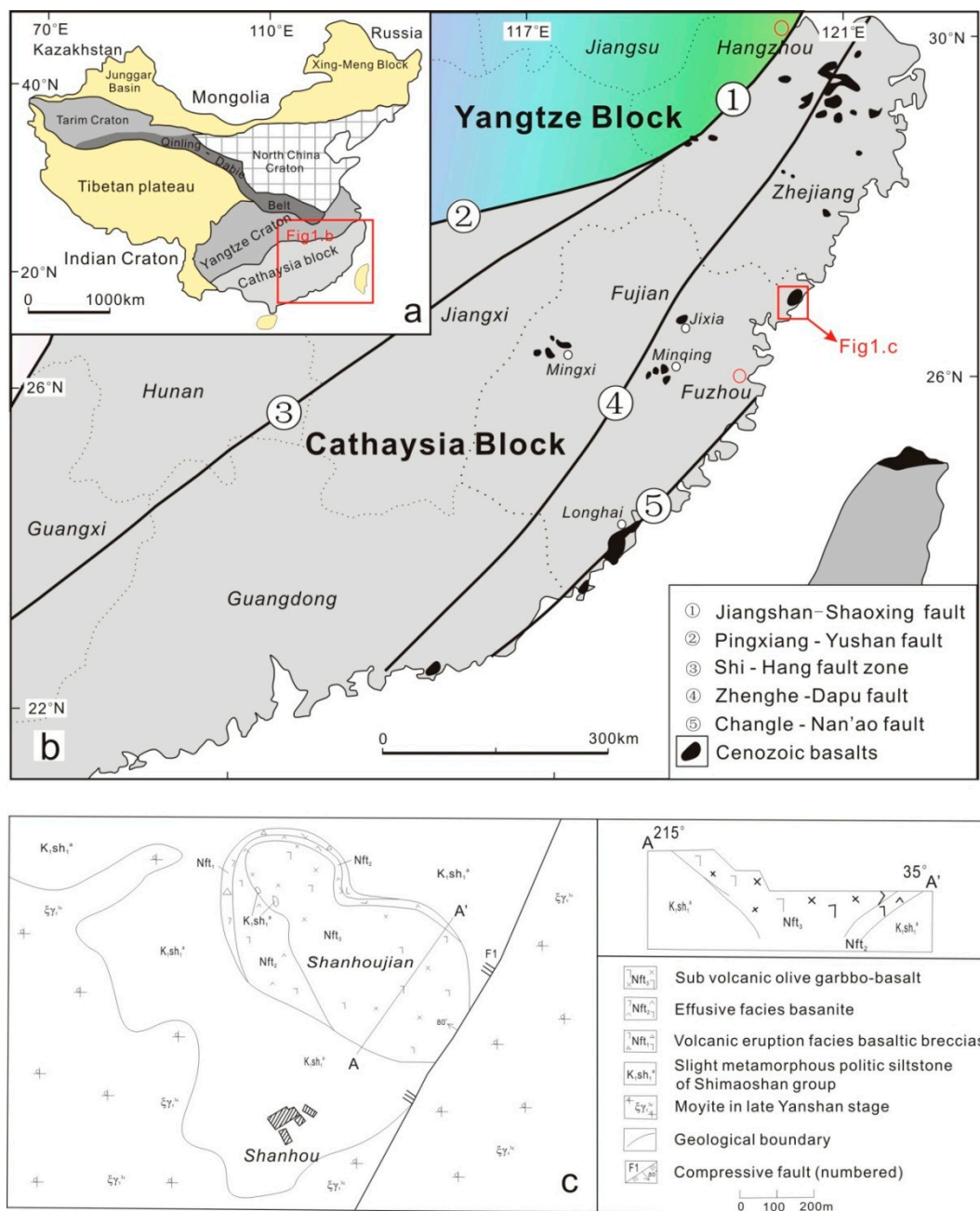
Figure 1. (**a**) Schematic geological map of China; (**b**) simplified geological map of Southeast (SE) China showing different tectonic domains (modified after [17,26]); (**c**) simplified geological map of the Shanhoujian district showing the distribution of volcanic rocks (modified after [22]).

The samples were collected from dark-gray subvolcanic olivine gabbro–basalts. The rock exhibits porphyritic texture with olivine, clinopyroxene, and plagioclase as the phenocrysts (Figure 2). Olivine (10–20 vol.%) is subhedral to anhedral with grain size ranging from 0.2 to 2 mm and shows cataclastic texture. Clinopyroxene (10–40 vol.%) is generally euhedral and prismatic with a gain size of 0.2–10 mm and exhibits a poikilitic texture with rounded olivine enclosed in clinopyroxene. The olivine inclusions are mainly distributed at the margins of clinopyroxene crystals. Plagioclase (25–35 vol.%) is euhedral and tabular with a grain size of 0.2–6 mm, exhibiting distinct polysynthetic twinning. The matrix (10–20 vol.%) is composed of clinopyroxene and plagioclase and basaltic glasses. Accessary minerals (~3 vol.%) include ilmenite, zircon, and apatite.
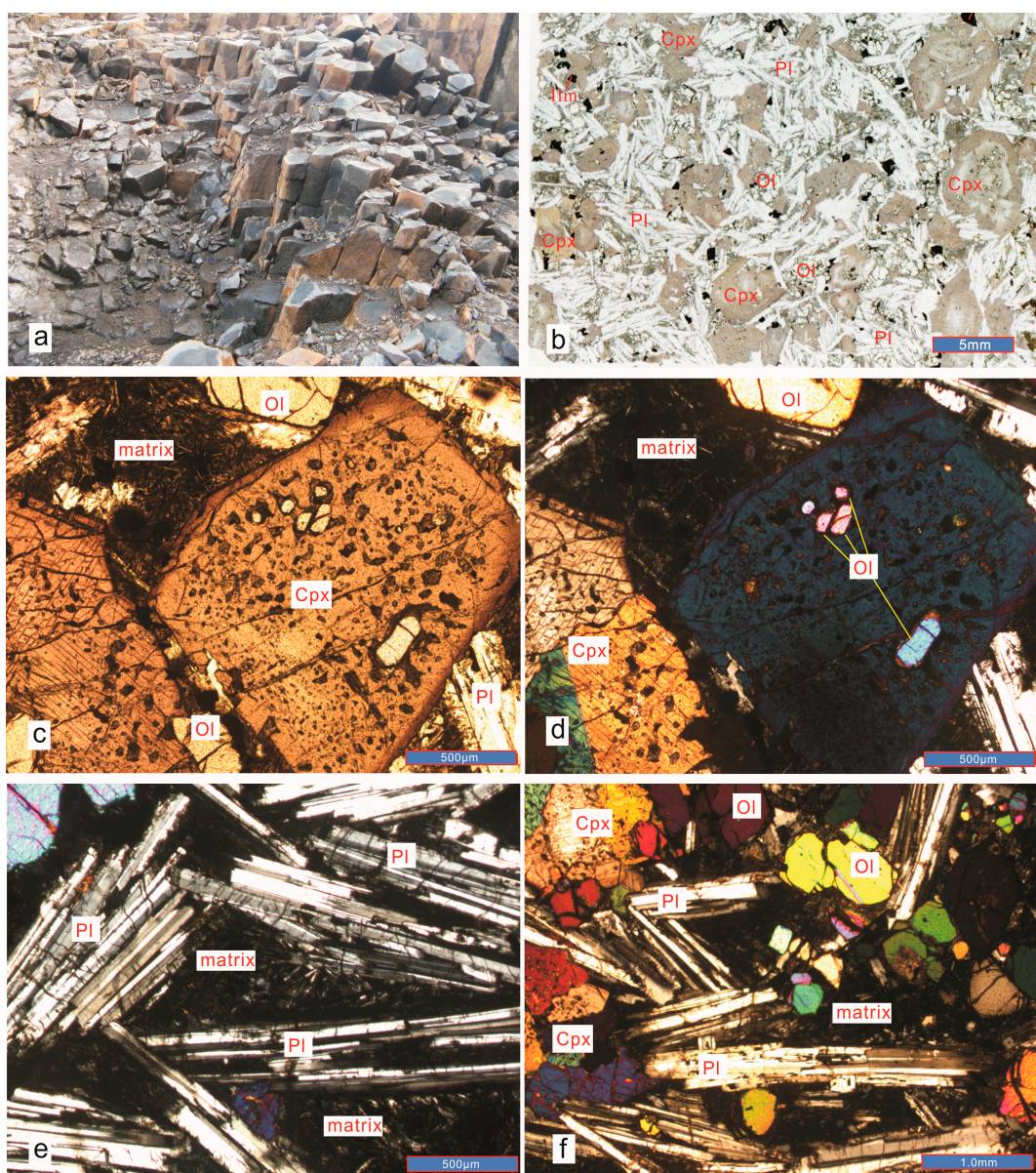
Figure 2. (**a**) Outcrop of Shanhoujian alkali basalts with columnar jointing. (**b**) Photomicrographs showing intergranular and porphyritic textures of Shanhoujian alkali basalts (taken in plane-polarized transmitted light); (**c**,**d**) fine-grained olivine enclosed by clinopyroxene (taken in plane-polarized and cross-polarized transmitted light, respectively); (**e**) tabular plagioclase and matrix forming hyalopilitic texture (taken in cross-polarized transmitted light); (**f**) anhedral to subhedral olivine interstitial to tabular plagioclase. Ol, olivine; Cpx, clinopyroxene; Pl, plagioclase; Ilm, Ilmenite.

3. Analytical Methods

3.1. Zircon U-Pb Dating

Zircon LA-ICP-MS U-Pb dating in this study was performed at the State Key Laboratory of Continental Dynamics, Northwest University. Based on petrographic observation, the zircon grains were separated using conventional gravity and magnetic separation methods and then handpicked under a binocular microscope. The selected zircon grains were mounted on epoxy resin and were polished to expose the internal texture. The samples were cleaned before dating analysis using a 3 vol.% HNO_3 solution to eliminate any surface contamination. After taking photographs under transmitted and reflected light, cathodoluminescence (CL) imaging was conducted with a Mono CL3+ CL system.

At the State Key Laboratory of Continental Dynamics, a laser ablation system (GeoLas200M) coupled with an inductively coupled plasma mass spectrometer (Agilent 7500a) was used for zircon U-Pb dating. During analysis, synthetic glass NIST 610 was used to optimize the instruments, and zircon standard 91500 was used as the external standard to monitor the status of the instrument. The detailed setup of the relevant parameters and the analytical protocol followed [27]. The raw data were then processed using Glitter software (version 4.0) by Macquarie University. The weighted mean age was calculated using Isoplot (version 4.16). Analyses with >10% discordance were excluded for the age calculations. The samples determined in this paper were formed in the Eocene, and the result was calculated at $^{206}Pb/^{238}U$ age. The isotopic ratios and age are expressed at 1σ.

3.2. Whole-Rock Major and Trace Elements

Rock samples were pulverized down to 200 mesh in an agate mortar. The rock powder samples were analyzed for major element contents using X-ray fluorescence (XRF; Shimazu 1800) at the Key Laboratory of Western China's Mineral Resources and Geological Engineering, Chang'an University, Xi'an China. The precision of the analysis was estimated to be better than ±2% (relative) for major elements with concentrations greater than 0.5 wt.% and ±5% (relative) for minor elements with concentrations greater than 0.1 wt.%. Whole-rock trace element concentrations were determined using ELAN–DRC-e ICP-MS at the State Key Laboratory of Ore Deposit Geochemistry Institute of Geochemistry, Chinese Academy of Sciences, Guiyang. The relevant precision was estimated to be better than ±5%. The detailed analytical procedure can be found in [28].

3.3. Whole-Rock Sr-Nd Isotopic Analysis

Whole-rock Sr–Nd isotopic ratios were obtained using a Finnigan Triton multi-collector mass spectrometer at the State Key Laboratory of Isotope Geochemistry Institute of Geochemistry, Chinese Academy of Sciences, Guangzhou, China. The mass fractionation corrections for Sr and Nd isotopic ratios are based on $^{86}Sr/^{88}Sr = 0.1194$ and $^{146}Nd/^{144}Nd = 0.7219$, respectively. The $^{87}Sr/^{86}Sr$ ratio of the NBS987 Sr standard and $^{143}Nd/^{144}Nd$ ratio of the La Jolla Nd standard determined using the same analytical procedure in this study were 0.710248 and 0.512115, respectively [29].

4. Results

4.1. Zircon U-Pb Dating Results

Thirty zircon grains were separated and collected from about 20 kg samples of Shanhoujian alkali basalts. Zircon grains are mainly euhedral and show prismatic morphology with grain size in the range of 50–120 μm. Zircon CL images and analyzed spots are shown in Figure 3.

Zircon U-Pb geochronological data are given in Table S1. Twenty-eight analyses from 28 zircon grains were obtained. After removing analyses showing strongly discordant ages, the dating result exhibited two age groups, one showing a weighted mean age of 117.5 ± 5.9 Ma (MSWD = 14) (Figure 4a) and the other an age of 40.10 ± 0.45 Ma (MSWD = 0.15) (Figure 4b). The latter was assumed to be the formation age of the alkali basalts, whereas the former probably represents the age of early Cretaceous magmatic rocks, consistent with late Mesozoic magmatism.

Figure 3. Cathodoluminescence images of representative zircon grains from Shanhoujian alkali basalts, the numbers in this figure is analysis spot number.
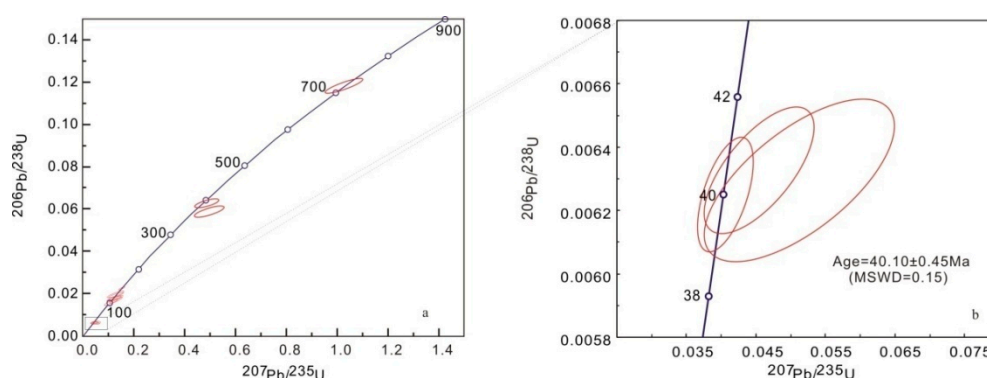

Figure 4. Zircon U–Pb concordia diagram for Shanhoujian alkali basalts in northeast Fujian. (**a**) group 1; (**b**) group 2.

4.2. Geochemical Characteristics

4.2.1. Major Elements

The results of the whole-rock major and trace elements analyses are listed in Table S2. The SiO_2, MgO, TFe_2O_3, and Al_2O_3 contents of the alkali basalts varied in ranges of 46.03–46.85 wt.%, 8.55–10.55 wt.%, 11.99–12.57 wt.%, and 11.23–13.19 wt.%, respectively. The Rittmann index (σ) ranged from 4.5 to 7.21 with an average value of 5.92 (>3.3), indicating that these rocks belong to the alkaline series.

The samples of the Shanhoujian alkali basalts show an alkaline trend in the SiO_2-K_2O+Na_2O diagram (Figure 5a), and are plotted along the boundary between alkaline basalts and basanite/nephelinite in Nb/Y-Zr/TiO_2 diagram (Figure 5b). The Na_2O/K_2O ratio varies in the range of 1.39–1.69 (1.52 on average), plotted in the K-series in the Na_2O-K_2O diagram. The MgO content shows a negative correlation with SiO_2, Al_2O_3, K_2O, P_2O_5, and TiO_2 and a positive correlation with CaO content and Cr concentration. However, the MgO content is scarcely correlated with TFeO, Ni, and Na_2O (Figure 6). The geochemistry of these rocks is reasonably consistent with the Cenozoic alkaline basalts in SE China.
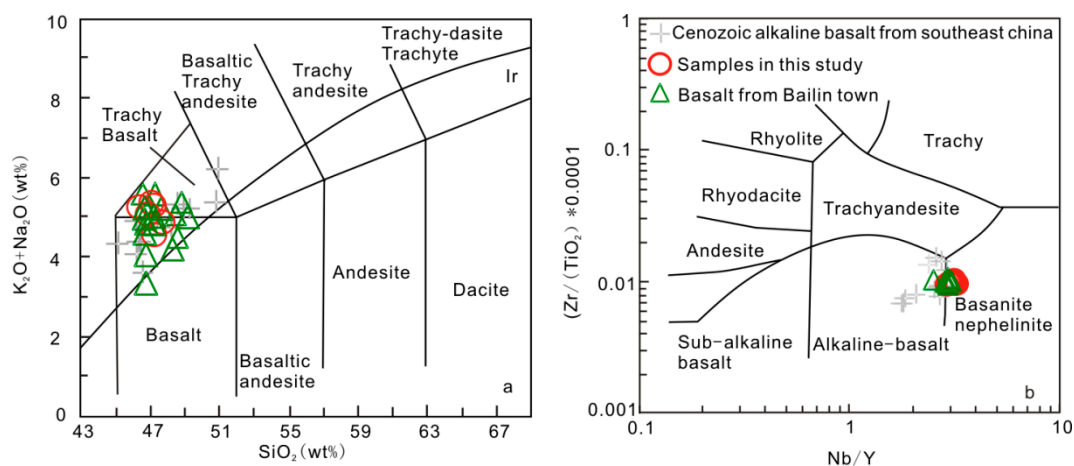
Figure 5. (**a**) (K₂O+Na₂O)-SiO₂ (after [30]) and (**b**) (Zr/TiO₂) ×0.0001-Nb/Y (after [31]) of alkali basalt from Shanhoujian in northeast Fujian. Data for basalts in Bailin are cited from [22,32] and for Cenozoic alkali basalts in southeast China from [17,20].
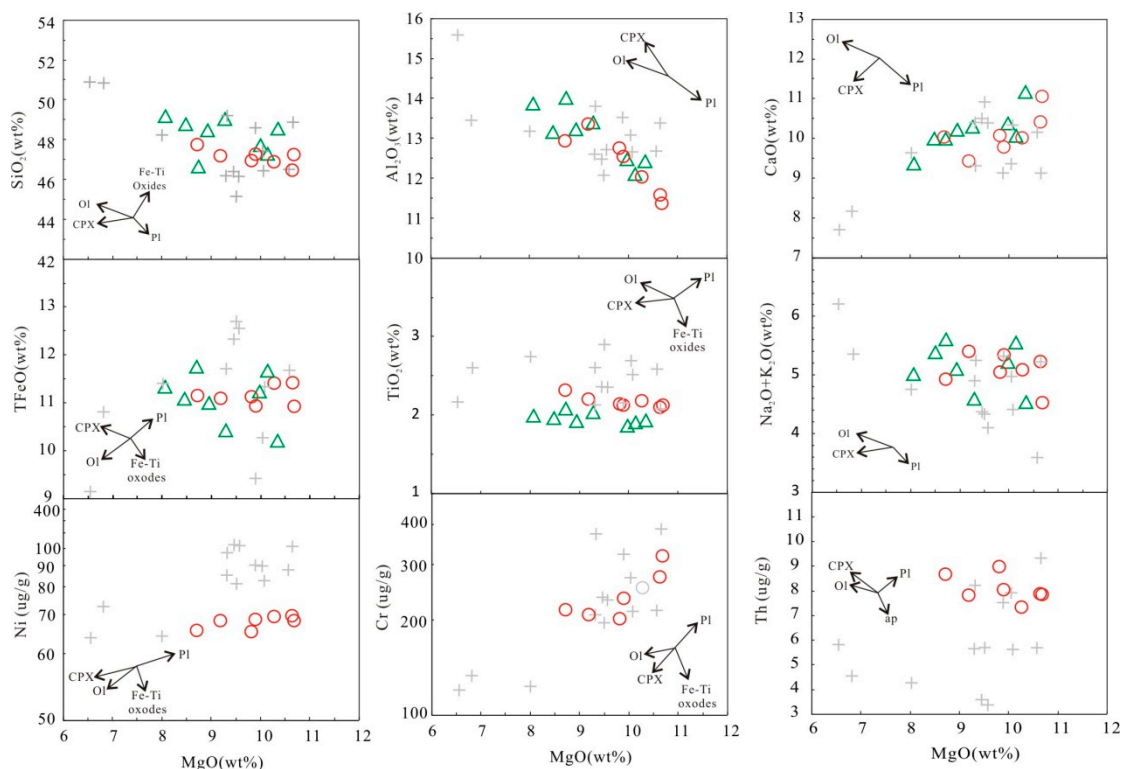

Figure 6. MgO Harker diagrams for alkali basalts from Shanhoujian in northeast Fujian (symbols and data are same as in Figure 5a).

4.2.2. Trace Elements and Rare Earth Elements

The trace element and rare earth element (REE) concentrations of the Shanhoujian alkali basalts are given in Table S2. Total REE concentrations range from 205 to 222 ppm, with an average value of 215 ppm. Light REE (LREE) is obviously fractionated from heavy REE (HREE), as indicated by the LREE/HREE ratio of 10.3–11.6 and C1-nomalized (La/Yb)$_N$ of 20.9–24.1. Eu/Eu* varies between 0.99 and 1.03 (1.01 on average), and Ce/Ce* is 0.92–0.94 (0.93 on average). The Cl-normalized REE patterns of the Shanhoujan alkali basalts are consistent with those of ocean island basalts (OIBs) and Cenozoic alkali basalts (Figure 7a).
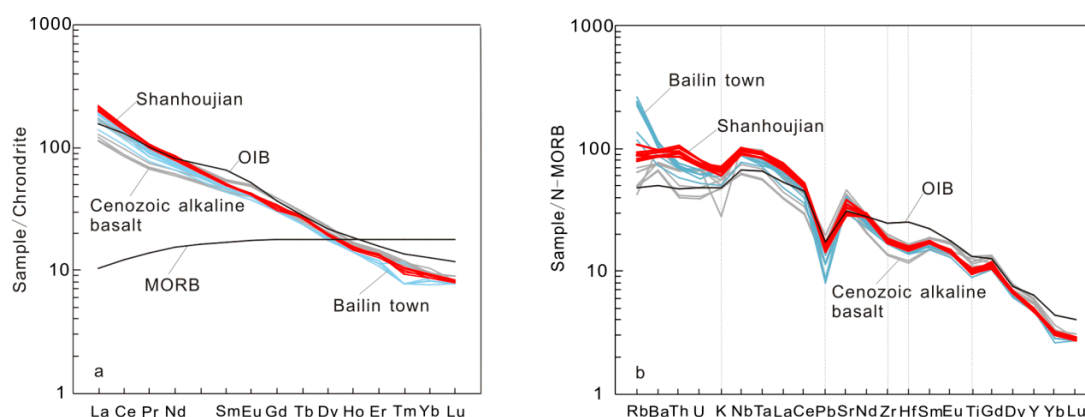
Figure 7. (**a**) Chondrite-normalized rare earth element patterns; (**b**) normal mid-ocean ridge basalt (N-MORB)-normalized spidergrams for alkali basalts from Shanhoujian in northeast Fujian. Element concentrations of chondrite, N-MORB, ocean island basalt (OIB), and MORB are cited from [33]. Data for Bailin basalts are from [32], and data of Cenozoic alkaline basalts from [17,20].

The N-MORB normalized trace element spidergram shows a right declined trend with decreasing incompatibility of trace elements. The spidergram also exhibits enrichment in Rb, Ba, Nb, and Ta and depletion in U, K, Pb, Zr, and Hf, with most samples showing slightly negative Ti anomalies (Figure 7b). Additionally, Ni and Cr concentrations vary from 126–147 ppm (138 ppm on average) and 202–308 ppm (243 ppm on average), respectively.

4.2.3. Sr-Nd Isotopic Compositions

The Sr-Nd isotopic compositions of the Shanhoujian alkali basalts are given in Table S3. The samples show low initial $(^{87}Sr/^{86}Sr)_i$ values ranging from 0.70406 to 0.70423 and initial $(^{143}Nd/^{144}Nd)_i$ values ranging from 0.512752 to 0.512752, with ε_{Nd} (40 Ma) varying between 3.2 and 3.3. Two samples are plotted in the field of OIB and Fujian Cenozoic volcanic rocks in the $(^{143}Nd/^{144}Nd)_i$–$(^{87}Sr/^{86}Sr)_i$ diagram (Figure 8), indicating that the Cenozoic alkali basalts in Fujian Province may have a mantle source with similar composition.

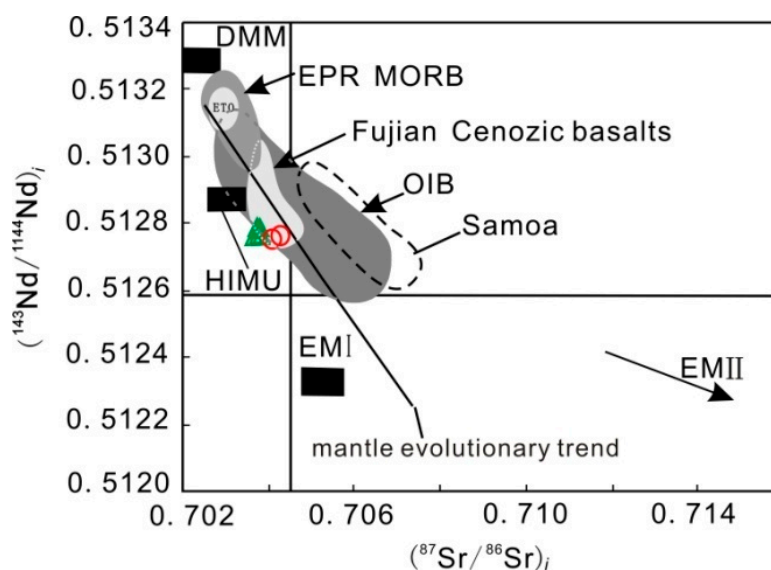**Figure 8.** $(^{143}Nd/^{144}Nd)_i$–$(^{87}Sr/^{86}Sr)_i$ of alkaline basalts from Shanhoujian in northeast Fujian. EMI (enriched mantle-type I), EMII (enriched mantle-type II), DMM (depleted mantle), and HIMU (high μ ratio mantle) from [34]; EPR (east pacific rise), MORB, and OIB from [35]; data of Fujian Cenozoic basalts from [6,17]. Symbols and data are same as in Figure 5a.

5. Discussion

5.1. Formation Age

Dai and Chen (2008) reported a 12 Ma age for the Shanhoujian alkali basalts but did not mention the detailed dating method [22]. For this paper, a 40.10 ± 0.45 Ma age for the Shanhoujian alkali basalts was obtained using zircon LA-ICP-MS U-Pb dating, indicating that the Shanhoujian alkali basalts resulted from an early Tertiary magmatism. Whole-rock ^{39}Ar-^{40}Ar analyses yielded an age of 33 Ma for the Shanhoujian alkali basalts (Ran Wang, personal communication). Because the blocking temperature for the U-Pb isotopic system in zircon is significantly higher than that of the whole-rock ^{39}Ar-^{40}Ar isotopic system and is more resistant to alteration and weathering, the zircon U-Pb age is likely more reliable.

Ho et al. (2003) subdivided the Cenozoic alkali basalts in Zhejiang-Fujian into Xiamen-Longhai (15–17 Ma), Minqing (12 Ma), and Mingxi-Changting (2.2–0.9 Ma) volcanic belts from the coastline inward [17]. Although the Shanhoujian alkali basalts are spatially distributed in the Xiamen-Longhai volcanic belt, the obtained U-Pb Zircon age is inconsistent with the age of the volcanic belt proposed by Ho et al. (2003) [17]. We propose that multiple volcanisms may have occurred in the Xiamen-Longhai volcanic belt.

In general, the mantle magmatism in SE China in the Cenozoic mainly occurred between 60 and 40 Ma. Mantle magmatism was probably absent in the period of 40–20 Ma, until it was activated again in this area after 20 Ma [17,18,36]. Recently obtained age data, however, show that mantle magmatism was still active in the period of 40–20 Ma, with Quzhou in Zhejiang Province (26.4 Ma), Songxi in Fujian Province (25 Ma), and NW and SE Taipai (23 Ma) [17] as representative examples. Zircon U-Pb dating results in this paper provide new evidence for volcanism from 40 to 20 Ma.

5.2. Fractional Crystallization and Crustal Contamination

5.2.1. Fractional Crystallization

The MgO and Ni contents of the Shanhoujian alkali basalts vary from 8.02 to 10.54 wt.% and from 126 to 147 ppm, respectively. The MgO content also shows a weak correlation with Ni (Figure 6), indicating weak or no fractionation of olivine during magma evolution. The primitive magma did not experience crystal fractionation involving plagioclase, as indicated by no negative Eu/Eu* anomaly and Ba enrichment of the basalts (Figure 7b). The samples exhibited a weakly positive correlation between CaO/Al_2O_3 and MgO and Cr and CaO, indicating a certain amount of pyroxene fractionated from the parental magmas [37]. Weak crystal fractionation indicates that the composition of the parental magmas did not significantly change.

5.2.2. Crustal Contamination

The occurrence of a few mantle xenoliths within the Shanhoujian basalts indicates that the parental magma migrated at a high speed without retention in the crust, and therefore was less contaminated by crustal materials. In addition, the geochemistry of the Shanhoujian alkali basalts does not support crustal contamination for the following reasons: (1) ^{87}Sr/^{86}Sr ratio shows no positive correlation with $1/^{86}Sr$ (Figure 9a). (2) Negative Pb anomalies shown in Figure 7b similar to OIB and MORB rule out the possibility of crustal contamination. (3) The continental crust has high Ba/Nb and La/Nb ratios [38], whereas mantle-derived basalts are characterized by relatively low ratios. In the plot of Ba/Nb vs. La/Nb, the two ratios of the Shanhoujian basalts show no correlation and the data point plot between PM (primitive mantle) and OIB (Figure 9b) is indicative of limited contamination related to crustal materials. (4) Mantle-derived basalts have a higher Nb/U ratio (47 ± 10) [39] than the crustal value (6.15) [38]. Moreover, the Shanhoujian basalts have an Nb/U ratio of 43.7 ± 1.4, similar to mantle-derived basalts. Therefore, the geochemical characteristics of the Shanhoujian alkali basalts are an efficient indicator of their mantle source and magma evolution.
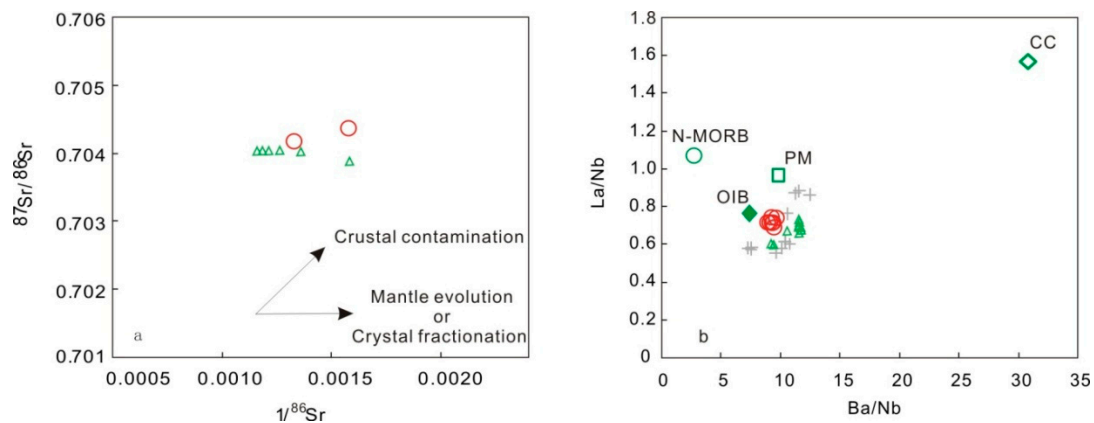
Figure 9. (**a**) $1/^{86}Sr$-$^{87}Sr/^{86}Sr$ plot and (**b**) Ba/Nb-La/Nb plot of alkaline basalt from Shanhoujian in northeast Fujian. Symbols and cited data are the same as in Figure 5a. Data for N-MORB and PM from [33], data for continental crust (CC) from [38].

5.3. Mantle Source

The Shanhoujian alkali basalts exhibit Sr-Nd isotopic compositions similar to that of OIB (Figure 8). Additionally, the incompatible trace element patterns of the Shanhoujian basalts are similar to that of OIB, except Zr, Hf, and Ti (Figure 7b). OIBs likely derived from low-degree partial melting of the asthenospheric mantle. Zr, Hf, Sm, and Eu have similar partition coefficients and therefore would not show strong fractionation from each other during partial melting of garnet peridotite mantle [40]. Similarly, Ti and Gd would also show no obvious fractionation due to their consistent partitioning behavior. The Shanhoujian basalts, however, display noticeable depletion in Zr, Hf, and Ti, suggesting that they were unlikely to have derived from partial melting of garnet peridotite mantle. Experimental studies suggest that carbonated peridotite, Si-unsaturated pyroxenite, and hornblendite would produce alkaline basaltic magmas and are possible mantle sources for alkali basalts [10–12,14,41]. Therefore, carbonated peridotite, Si-unsaturated pyroxenite, and hornblendite are possible mantle sources for the Shanhoujian alkali basalts.

5.3.1. Hornblendite

The Shanhoujian alkali basalts are geochemically similar to the hornblendite-derived melts, which show enrichment in Ba, La, and Nb and depletion in U, Zr, Hf, K, and Pb. The Shanhoujian basalts, however, are different from hornblendite-derived melts in terms of Ti content and Fe/Mn and Ba/Rb ratios. The Shanhoujian basalts show a different evolutionary path from the hornblendite-derived basaltic magmas in the plot of $Na_2O + K_2O$ vs. TiO_2 (Figure 10). This indicates that there was no obvious contribution from hornblendite-derived melts.

The Fe/Mn ratio is efficient in constraining the mantle source of alkali basalts [42,43]. The Shanhoujian basalts show a Fe/Mn ratio of 64.3 ± 3.4, higher than that of hornblendite-derived melts (Fe/Mn = 55.8 ± 6.9) [41]. In addition, the Shanhoujian basalts have a higher Rb/Sr ratio (0.075–0.083) and lower Ba/Rb ratio (10.0–11.9) than hornblendite-derived melts (Rb/Sr < 0.1; Ba/Rb > 20) [41,44]. These geochemical features collectively suggest that mantle hornblendite is not likely to have been the mantle source of the Shanhoujian alkali basalts.
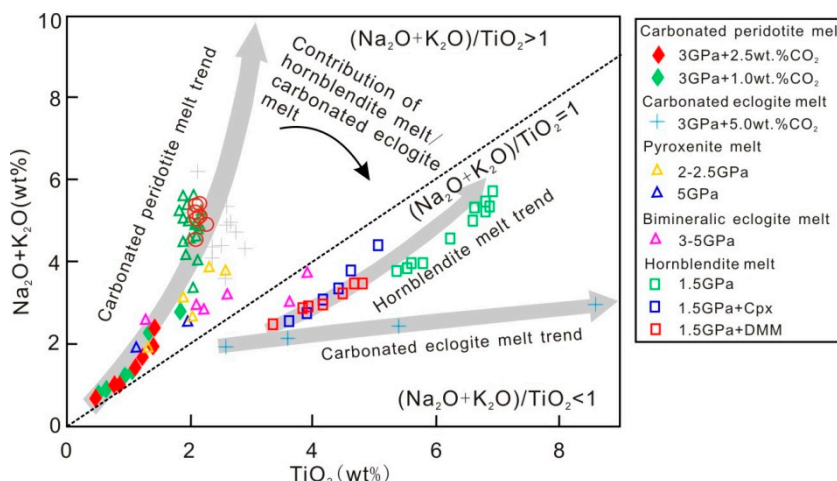
Figure 10. (K_2O + Na_2O)-TiO_2 plot of alkaline basalt from Shanhoujian in northeast Fujian (after [45]; symbols and data are same as in Figure 5a).

5.3.2. Pyroxenite

The Fe/Mn, Fe/Zn, La/Nb, and Sr/Nd ratios of melts derived from partial melting of mantle pyroxenite and peridotite are important indicators of the composition of the mantle source. The ratio of partition coefficients of Fe/Mn ($D_{Fe/Mn}$) between pyroxene and garnet is smaller than 1, whereas that of olivine is greater than 1 [43]. Also, the primitive basaltic magmas derived from partial melting of mantle pyroxenites and peridotites commonly have a different Fe/Mn ratio (Figure 11a,b). Regardless of the anhydrous or hydrous system, the Fe/Mn ratio of the primary magmas derived from mantle peridotites has a relatively weak correlation with the MgO and MnO contents in comparison to the mantle pyroxenites. For example, MORB has a Fe/Mn ratio of 53.1 ± 2.3 (MgO > 5.5%) [46]. The Shanhoujian alkali basalts have a Fe/Mn ratio of 64.3 ± 3.4, consistent with magmas derived from partial melting of mantle pyroxenites including the alkali basalts in East China (Fe/Mn = 68.6 ± 11.5) [42] and OIB (Fe/Mn = 63.4 ± 6.9) (Figure 11a,b). Therefore, the Shanhoujian alkali basalts are supposedly derived from the mantle source dominated by pyroxenite components, as indicated by the high Fe/Mn ratio.
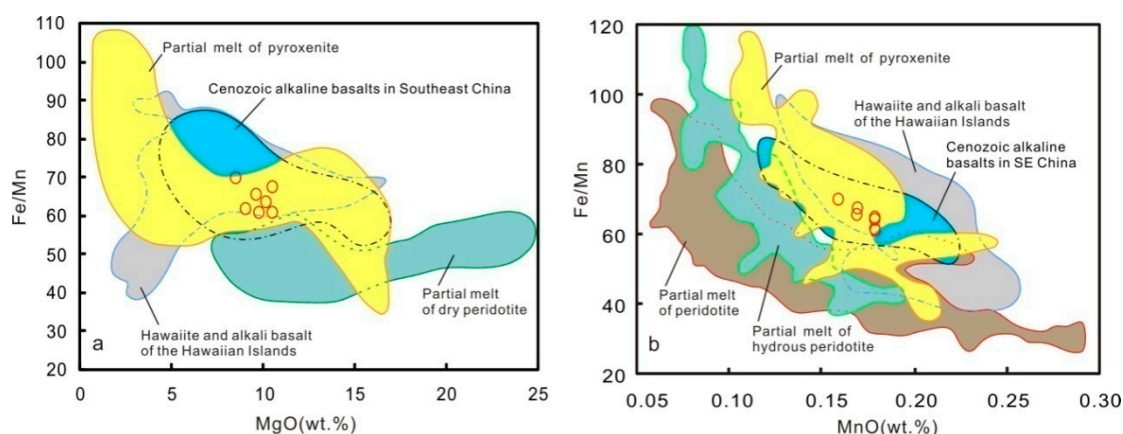

Figure 11. Binary plots of (**a**) MgO vs. Fe/Mn and (**b**) MnO vs. Fe/Mn (after [20]). Symbols as in Figure 5a. Data of Hawaii from GEOROC (http://georoc.mpch-mainz.gwdg.de/georoc/Start.asp), and of SE China from [17,20].

Experimental studies indicate that $D_{Fe/Zn}$ approximates 1 for olivine and orthopyroxene, and the value for clinopyroxene and garnet is much larger than 1 [43,47,48]. Thus, melts derived from mantle pyroxenites should have a lower Fe/Zn ratio than those derived from mantle peridotites. The Fe/Zn ratio

of the Shanhoujian alkali basalts is 678 ± 34, lower than that of MORB (930–1200) [47], indicating that the mantle source should contain pyroxenite components [49].

The La/Nb ratio of the primary magmas derived from mantle pyroxenite is lower than that of the pyroxenite source, whereas the Sr/Nd ratio is higher than that of the source pyroxenite due to different partition coefficients of La, Nb, Sr, and Nd between pyroxenite and melts ($D_{La/Nb}$ = 2.92; $D_{Sr/Nd}$ = 0.346) [50]. Experimental studies have demonstrated that mantle pyroxenite is the predominant component of the mantle source for OIB [51]. High ^{143}Nd/^{144}Nd and Sr/Nd ratios along with La/Nb < 1 indicate that alkali basalts are derived from mantle pyroxenites [52]. The La/Nb (0.71 ± 0.02) and Sr/Nd (17.8 ± 1.6) ratios are similar to those of OIB (La/Nb = 0.84 ± 0.12; Sr/Nd = 18.4 ± 4.6). They define a trend indicative of the addition of a mantle pyroxenite component in the La/Nb vs. Sr/Nd plot (Figure 12). The high Nd isotopic composition (0.512752–0.512756) also indicates the presence of pyroxenite in the mantle source for the Shanhoujian alkali basalts.
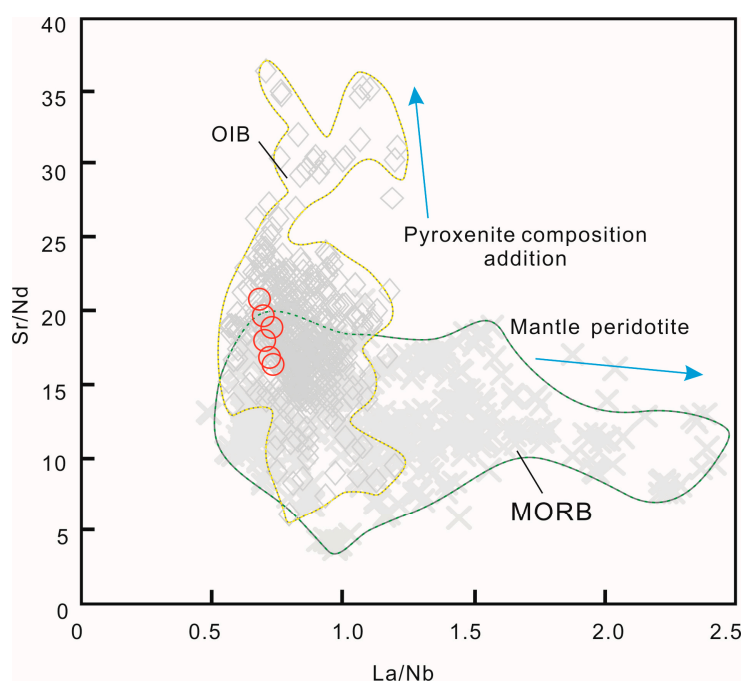

Figure 12. Binary plot of La/Nb-Sr/Nd for Shanhoujin alkali basalts (symbols as in Figure 5a). Data of OIB (La/Nb = 0.84 ± 0.12, Sr/Nd=18.4 ± 4.6, *n* = 396) from GEOROC (http://georoc.mpch-mainz.gwdg.de/georoc/Start.asp), and of MORB (La/Nb = 1.15 ± 0.42, Sr/Nd = 12.6 ± 3.8, *n* = 490) from [46].

The partition coefficient ratio of $D_{La/Nb}$ and $D_{Sr/Nd}$ for peridotite-melt is approximately 1. Therefore, element pairs La-Nb and Sr-Nd scarcely fractionate and the La/Nb and Sr/Nd ratios of mantle-derived magmas are theoretically equal to or slightly larger than those of their mantle sources. For instance, MORB (La/Nb = 1.15 ± 0.42; Sr/Nd = 12.6 ± 3.8) [46] commonly resembles its mantle source (La/Nb = 1.11; Sr/Nd = 13.74) [53]. The trend defined by the La/Nb and Sr/Nd ratios is opposite to that of MORB (Figure 12), which suggests that mantle peridotite is not a major component of the mantle source for the Shanhoujian alkali basalts.

5.3.3. Carbonated Mantle Peridotite

Experiments on partial melting of carbonated peridotite indicate that alkaline basaltic magmas can be derived from low-degree partial melting of CO_2-bearing mantle lherzolite [10,54]. Such magma would inherit the geochemical characteristics of carbonated mantle [9] that shows enrichment in the majority of incompatible trace elements, especially LREE, and depletion in K, Zr, Hf, and Ti [55]. The Shanhoujian alkali basalts are characterized by distinct depletion in K, Zr, Hf, and Ti (Figure 7b).

The samples define a trend along a line showing partial melting of the carbonated peridotite in the Na_2O+K_2O vs. TiO_2 plot. This phenomenon, along with the LREE enrichment (($La/Yb)_N$ = 20.9–24.1), suggests that the Shanhoujia alkali basalts were derived from a mantle source containing carbonated peridotite. The degree of depletion in Zr, Hf, and Ti of the Shanhoujian alkali basalts is lower than that in Shandong Province [9]. This geochemical signature can be explained by the fact that the depletion in Zr, Hf, and Ti is commonly offset by the addition of mantle pyroxenite components to various extents during partial mantle melting.

The Shanhoujian alkali basalts were most likely derived from a source containing both pyroxenite and carbonated peridotite, as indicated by high Fe/Mn and Fe/Zn ratios, a low La/Nb ratio, and depletion in Zr, Hf, and Ti.

6. Tectonic Implications

The Shanhoujian alkali basalts are part of the volcanic belt in SE China and were formed in the Eocene (40 Ma). In the plot of 2 × Nb-Zr/4-Y vs. Ta/Hf-Th/Hf, all samples are plotted in the field of intraplate rift tectonic settings (Figure 13).

The Cenozoic tectonic evolution of SE China is closely related to the subduction of the Pacific plate, extension of the South Sea, the subduction and collision of the Philippines plate, and the tectonic activity of the Neo-Tethys. The Shanhoujian alkali basalts formed in the Eocene, but the extension of the South Sea and the subduction of the Philippines plate postdated the Eocene epoch. Therefore, the formation of the Shanhoujian alkali basalts was not caused by the subduction of the Pacific plate and tectonic activity of the Neo-Tethys. After the Izanagi plate completely subducted beneath the Eurasia plate, the subduction of the Pacific plate beneath the Eurasia plate became a high-angle subduction and the velocity rapidly decreased due to the plate rollback [56]. During this period, the Tethys Ocean in SW China closed and the Indian plate collided with the Eurasia plate and then underwent uplift and orogenesis, resulting in NE- and NNE-trending dextral strike-slip faults in east China. The subduction and orogenesis resulted in an extensional tectonic setting in SE China, forming a series of dextral extensional faulted basins (such as Sanshui basin in Guangdong Province) that were characterized by active volcanism. Accompanied by plate rollback, the Pacific plate subducted obliquely at a high angle, which resulted in vertical or more complex asthenospheric convection and upwelling that later led to extension and thinning of the continental lithosphere [56].

At the early stage, the subduction of the Pacific plate was more than 1000 km inland. At the late stage, the subduction angle increased and the plate retreated. Geophysical data show that some residual subducted slab was retained in the mantle transitional zone [57], suggesting that the ancient Pacific plate entered into the transition zone. During the subduction of the ancient Pacific plate, the plates and sediments carried by them experienced extensive dehydration at different depths. The released silica-rich melts in the upper part of the subduction tunnel interacted with mantle wedge, causing serpentinization and cholritization. As the subduction depth increased, these metamorphosed crustal rocks underwent dehydration melting to produce hydrous melts and interacted with mantle-wedge peridotite, forming silica-unsaturated pyroxenite [16]. Meanwhile, the carbonates carried by the subducted slab were injected to a depth of 300–400 km [58] or even deeper [54]. The carbonates would have melted to form carbonate melts at high pressure and reacted with mantle peridotite [59], forming carbonated peridotite with vein-like stockwork and pudding-like carbonates [60–62].
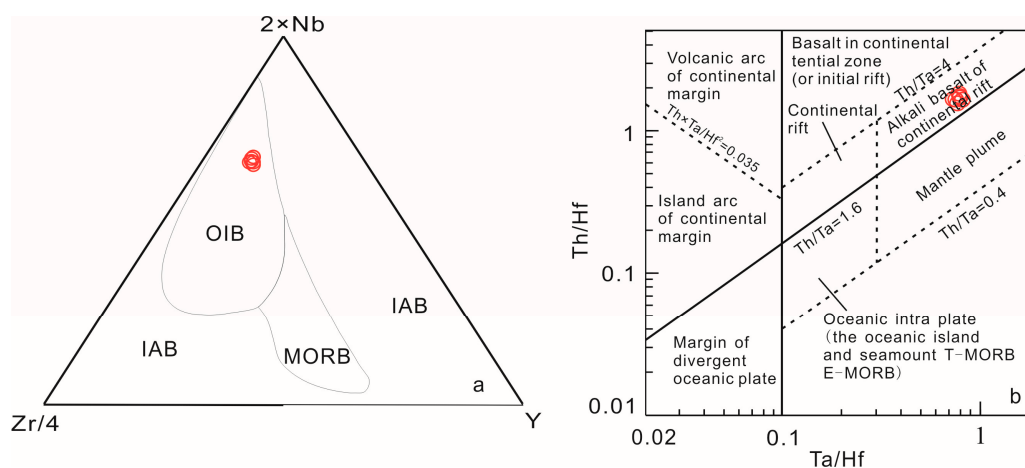
Figure 13. (**a**) Ternary diagram of 2×Nb-Zr/4-Y (after [63]) and (**b**) binary diagram of Ta/Hf-Th/Hf (after [64]), showing tectonic setting of Shanhoujian alkali basalts. IAB, island arc basalt; OIB, ocean island basalt; MORB, mid-ocean ridge basalt.

With the closure of the new Tethys Ocean, the collision between the India and Eurasian plates resulted in the formation of the NE- and NNE-trending dextral strike-slip faults in east China [56]. The Pacific plate rollback caused lithospheric thinning and large-scale extension in SE China. Under the influence of the Pacific and Tethys tectonic system, the NE- and NEE-trending extension belts were formed, which controlled the distribution of Cenozoic volcanic rocks. The asthenospheric mantle upwelled along the weak zones and led to further extension in SE China to form a continental rift setting. The pyroxenite and carbonated peridotite carried by the asthenospheric mantle underwent partial adiabatic decompression melting to form primitive alkaline basaltic magmas (Figure 14). Therefore, we interpret that the Shanhoujian alkali basalts formed in a continental rift setting.
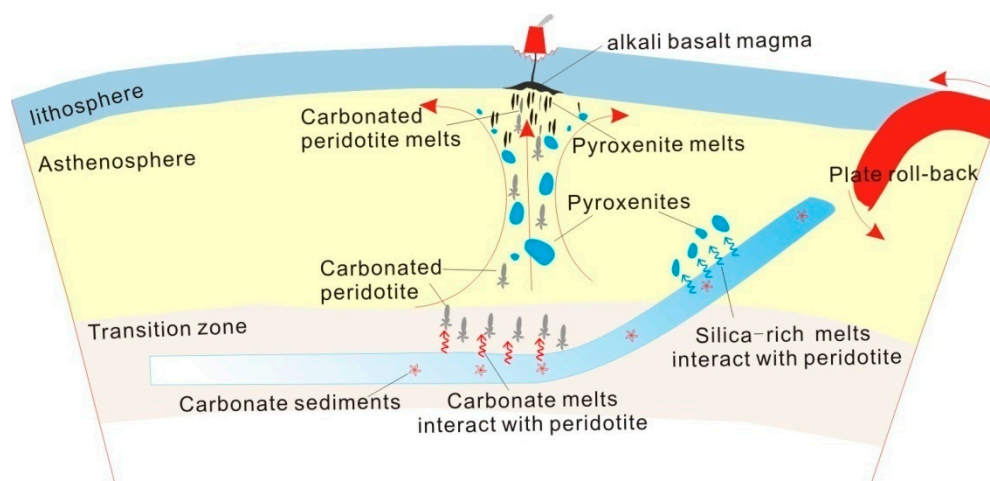

Figure 14. Schematic diagram showing the formation of Shanhoujian alkali basalt in northeast Fujian.

7. Conclusions

(1) Zircon U-Pb dating indicates that the Shanhoujian alkali basalts were emplaced at 40.10 ± 0.45 Ma.

(2) The geochemical characteristics of the Shanhoujian alkali basalts suggest that the parental magmas underwent insignificant crustal contamination and fractionation during emplacement. Therefore, they are an efficient indicator of their mantle source and magma evolution. The parental magma was derived from a mantle source containing pyroxenites and carbonated peridotites.

Partial melting of the mantle pyroxenites and carbonated peridotite carried during asthenospheric upwelling generated the primitive basaltic magmas that formed the Shanhoujian alkali basalts.

(3) The Shanhoujian alkali basalts formed in a continental rift setting. The continuous upwelling of the asthenospheric mantle led to further extension of lithosphere, forming a continental rift setting under control of NE (NNE)-trending extensional tectonism and Pacific-plate roll-back tectonism.

References

1. Hofmann, A.W. Sampling mantle heterogeneity through oceanic basalts: Isotopes and trace elements. In *Treatise on Geochemistry*, 1st ed.; Carlson, R.W., Ed.; Elsevier-Pergamon: Oxford, UK, 2003; Volume 2, pp. 61–101.

2. White, W.M. Oceanic island basalts and mantle plumes: The geochemical perspective. *Annu. Rev. Earth Plant. Sci.* **2010**, *38*, 133–160. [CrossRef]

3. Niu, Y.L.; Hara, M.J.O. Origin of ocean island basalts: A new perspective from petrology, geochemistry, and mineral physics considerations. *J. Geophys. Res. Solid Earth* **2003**, *108*, 2209–2213. [CrossRef]

4. Pilet, S.; Hernandez, J.; Bussy, F.; Sylvester, P.J. Short-term metasomatic control of Nb/Th ratios in the mantle sources of intraplate basalts. *Geology* **2004**, *32*, 113–116. [CrossRef]

5. Upadhyay, D.; Jahn-Awe, S.; Pin, C.; Paquette, J.L.; Braun, I. Neoproterozoic alkaline magmatism at Sivamalai, southern India. *Gondwana Res.* **2006**, *10*, 156–166. [CrossRef]

6. Zou, H.B.; Zindler, A.; Xu, X.S.; Qi, Q. Major, trace element, and Nd, Sr and Pb isotope studies of Cenozoic basalts in SE China: Mantle sources, regional variations, and tectonic significance. *Chem. Geol.* **2000**, *171*, 33–47. [CrossRef]

7. Tang, Y.; Zhang, H.; Ying, J. Asthenosphere–lithospheric mantle interaction in an extensional regime: Implication from the geochemistry of Cenozoic basalts from Taihang Mountains, North China Craton. *Chem. Geol.* **2006**, *233*, 309–327. [CrossRef]

8. Chen, L.H.; Zeng, G.; Hu, S.L.; Yu, X.; Chen, X.Y. Crust recycling and genesis of continental alkaline basalts: Case study of the cenozoic alkaline basalts from shandong province, eastern china. *Geol. J. China Univ.* **2012**, *18*, 16–27. (In Chinese)

9. Zeng, G.; Chen, L.H.; Hofmann, A.W.; Jiang, S.Y.; Xu, X.S. Crust recycling in the sources of two parallel volcanic chains in Shandong, North China. *Earth Planet. Sci. Lett.* **2011**, *302*, 359–368. [CrossRef]

10. Dasgupta, R.; Hirschmann, M.M.; Smith, N.D. Partial melting experiments of peridotite CO_2 at 3 GPa and genesis of alkalic ocean island basalts. *J. Petrol.* **2007**, *48*, 2093–2124. [CrossRef]

11. Kogiso, T.; Hirschmann, M.M. Experimental study of clinopyroxenite partial melting and the origin of ultra-calcic melt inclusions. *Contrib. Mineral. Petrol.* **2001**, *142*, 347–360. [CrossRef]

12. Kogiso, T.; Hirschmann, M.M. Partial melting experiments of bimineralic eclogite and the role of recycled mafic oceanic crust in the genesis of ocean island basalts. *Earth Planet. Sci. Lett.* **2006**, *249*, 188–199. [CrossRef]

13. Dasgupta, R.; Hirschmann, M.M.; Stalker, K. Immiscible transition from carbonate-rich to silicate-rich melts in the 3 GPa melting interval of eclogite+ CO_2 and genesis of silica-undersaturated ocean island lavas. *J. Petrol.* **2005**, *47*, 647–671. [CrossRef]

14. Mallik, A.; Dasgupta, R. Reactive infiltration of MORB-eclogite-derived carbonated silicate melt into fertile peridotite at 3 GPa and genesis of alkalic magmas. *J. Petrol.* **2013**, *42–43*, 209–214. [CrossRef]

15. Huang, S.C.; Zheng, Y.F. Mantle geochemistry: Insights from oceanic island basalt. *Sci. China Earth Sci.* **2017**, *47*, 5–32. (In Chinese) [CrossRef]

16. Zheng, Y.F.; Chen, Y.X.; Dai, L.Q.; Zhao, Z.F. Developing plate tectonics theory from oceanic subduction zones to collisional orogens. *Sci. China Earth Sci.* **2015**, *58*, 1045–1069. (In Chinese) [CrossRef]

17. Ho, K.S.; Chen, J.C.; Lo, C.H.; Zhao, H.L. [40]Ar–[39]Ar dating and geochemical characteristics of late Cenozoic basaltic rocks from the Zhejiang–Fujian region, SE China: Eruption ages, magma evolution and petrogenesis. *Chem. Geol.* **2003**, *197*, 287–318. [CrossRef]

18. Zhang, G.S.; Wen, H.J.; Hu, R.Z.; Qiu, Y.Z. Geochemical features of the Cenozoic alkaline ultramafic volcanic rock in Fujian and their tectonic significance. *Acta Geol. Sin.* **2009**, *83*, 284–294. (In Chinese)

19. Yang, A.Y.; Zhao, T.P.; Qi, L.; Yang, S.H.; Zhou, M.F. Chalcophile elemental constraints on sulfide-saturated fractionation of Cenozoic basalts and andesites in SE China. *Lithos* **2011**, *127*, 323–335. [CrossRef]

20. Li, Y.Q.; Ma, C.Q.; Robinson, P.T.; Zhou, Q.; Liu, M.L. Recycling of oceanic crust from a stagnant slab in the mantle transition zone: Evidence from Cenozoic continental basalts in Zhejiang Province, SE China. *Lithos* **2015**, *230*, 146–165. [CrossRef]

21. Yang, Z.F.; Li, J.; Liang, W.F.; Luo, Z.H. On the chemical markers of pyroxenite contributions in continental basalts in Eastern China: Implications for source lithology and the origin of basalts. *Earth-Sci. Rev.* **2016**, *157*, 18–31. [CrossRef]

22. Dai, Q.Z.; Chen, R.K. On the geologic characteristics and formation mechanisms of the basalt pillars in Shanhoujian, Fuding City. *Geol. Fujian* **2008**, *27*, 369–376. (In Chinese)

23. Zhang, G.W.; Guo, A.L.; Wang, Y.J.; Li, S.Z.; Dong, Y.P.; Liu, S.F.; He, D.F.; Cheng, S.Y. Tectonics of South China Continent and its implications. *Sci. China: Earth Sci.* **2013**, *56*, 1804–1828. [CrossRef]

24. Charvet, J.; Shu, L.; Shi, Y.; Guo, L.; Faure, M. The building of south China: Collision of Yangzi and Cathaysia blocks, problems and tentative answers. *J. SE Asian Earth Sci.* **1996**, *3–5*, 223–235. [CrossRef]

25. Zhang, G.S.; Bobrov, A.V.; Long, J.S.; Han, W.H. Mineralogical and geochemical patterns of mantle xenoliths from the Jixia region (Fujian Province, southern China). *Geochem. Int.* **2016**, *54*, 901–913. [CrossRef]

26. Yu, Y.; Xu, X.S.; Griffin, W.L.; O'Reilly, S.Y.; Xia, Q.K. H_2O contents and their modification in the Cenozoic subcontinental lithospheric mantle beneath the Cathaysia block, SE China. *Lithos* **2011**, *126*, 182–197. [CrossRef]

27. Yuan, H.L.; Gao, S.; Dai, M.N.; Zong, C.L.; Günther, D.; Fontaine, G.H.; Liu, X.M.; Diwu, C.R. Simultaneous determinations of U–Pb age, Hf isotopes and trace element compositions of zircon by excimer laser-ablation quadrupole and multiple-collector ICP-MS. *Chem. Geol.* **2008**, *247*, 100–118. [CrossRef]

28. Qi, L. Determination of trace elements in granites by inductively coupled plasma mass spectrometry. *Talanta* **2000**, *51*, 507–513.

29. Liang, X.R.; Wei, G.J.; Li, X.H.; Liu, Y. Precise determination of [143]Nd/[144]Nd and Sm/Nd ratios using multiple-collectors inductively coupled plasma-mass spectrometer (MC-ICP-MS). *Geochimica* **2003**, *32*, 91–96. (In Chinese)

30. Le Maitre, R.W.; Bateman, P.; Dudek, A.; Keller, J.; Lameyre, J.; Le Bas, M.J.; Sabine, P.A.; Schmid, R.; Sorensen, H.; Streckeisen, A.; et al. *A Classification of Igneous Rocks and a Glossary of Terms*, 2nd ed.; Blackwell Scientific: Oxford, UK, 1989; pp. 32–36.

31. Winchester, J.A.; Floyd, P.A. Geochemical discrimination of different magma series and their differentiation products using immobile elements. *Chem. Geol.* **1977**, *20*, 325–343. [CrossRef]

32. Liu, S.C. Water Content and Geochemistry of the Cenozoic Basalts in SE China: Implications for Enrichment in the Mantle Source of Intra-Plate Basalts. Ph.D. Thesis, University of Science and Technology of China, Anhui, China, 2016.

33. Sun, S.S.; McDonough, W.F. Chemical and isotopic systematics of oceanic basalts: Implications for mantle composition and processes. *Geol. Soc. Lond. Spec. Publ.* **1989**, *42*, 313–345. [CrossRef]

34. Zindler, A.; Hart, S. Chemical geodynamics. *Annu. Rev. Earth Planet. Sci.* **1986**, *14*, 493–571. [CrossRef]

35. Wilson, B.M. *Igneous Petrogenesis a Global Tectonic Approach*, 10th ed.; Springer: Dordrecht, The Netherlands, 2007; pp. 245–374.

36. Zhu, B.Q.; Wang, H.F.; Chen, Y.W.; Chang, X.Y.; Hu, Y.G.; Xie, J. Geochronological and geochemical constraint on the Cenozoic extension of Cathaysian lithosphere and tectonic evolution of the border sea basins in East Asia. *J. Asian Earth Sci.* **2004**, *24*, 163–175.

37. Späth, A.; Le Roex, A.P.; Opiyo-Akech, N. Plume–Lithosphere interaction and the origin of continental rift-related Alkaline Volcanism—The Chyulu Hills volcanic province, southern Kenya. *J. Petrol.* **2001**, *42*, 765–787. [CrossRef]

38. Rudnick, R.L.; Gao, S. Composition of the continental crust. In *Treatise on Geochemistry*, 1st ed.; Holland, H.D., Turekian, K.K., Eds.; Elsevier-Pergamon: Oxford, UK, 2003; Volume 3, pp. 1–64.

39. Hofmann, A.W.; Jochum, K.P.; Seufert, M.; White, W.M. Nb and Pb in oceanic basalts: New constraints on mantle evolution. *Earth Planet. Sci. Lett.* **1986**, *79*, 33–45. [CrossRef]

40. Salters, V.J.M.; Longhi, J.E.; Bizimis, M. Near mantle solidus trace element partitioning at pressures up to 3.4 GPa. *Geochem. Geophys. Geosyst.* **2002**, *3*, 1–23. [CrossRef]

41. Pilet, S.; Baker, M.B.; Stolper, E.M. Metasomatized lithosphere and the origin of alkaline Lavas. *Science* **2008**, *320*, 916–919. [CrossRef]

42. Zhang, B.H.; Liu, Y.S.; Gao, S. Petrogenetic significance of high Fe/Mn ratios of the Cenozoic basalts from eastern China. *Sci. China (Ser. D)* **2007**, *37*, 1456–1466. (In Chinese) [CrossRef]

43. Le Roux, V.; Lee, C.T.A.; Turner, S.J. Zn/Fe systematics in mafic and ultramafic systems: Implications for detecting major element heterogeneities in the Earth's mantle. *Geochim. Cosmochim. Acta* **2010**, *74*, 2779–2796. [CrossRef]

44. Furman, T.; Graham, D. Erosion of lithospheric mantle beneath the East African Rift system: Geochemical evidence from the Kivu volcanic province. *Dev. Geotecton.* **1999**, *24*, 237–262.

45. Zeng, G.; Chen, L.; Xu, X.; Jiang, S.; Hofmann, A.W. Carbonated mantle sources for Cenozoic intra-plate alkaline basalts in Shandong. North China. *Chem. Geol.* **2010**, *273*, 35–45. [CrossRef]

46. Jenner, F.E.; O'Neill, H.S.C. Analysis of 60 elements in 616 ocean floor basaltic glasses. *Geochem. Geophys. Geosyst.* **2012**, *13*. [CrossRef]

47. Le, R.V.; Dasgupta, R.; Lee, C.T.A. Mineralogical heterogeneities in the Earth's mantle: Constraints from Mn, Co, Ni and Zn partitioning during partial melting. *Earth Planet. Sci. Lett.* **2011**, *307*, 408.

48. Lee, C.T.A.; Luffi, P.; Le Roux, V.; Dasgupta, R.; Albarede, F.; Leeman, W.P. The redox state of arc mantle using Zn/Fe systematics. *Nature* **2010**, *468*, 681–685. [CrossRef]

49. Sobolev, A.V.; Hofmann, A.W.; Sobolev, S.V.; Nikogosian, I.N. An olivine-free mantle source of Hawaiian shield basalts. *Nature* **2005**, *434*, 590–597. [CrossRef] [PubMed]

50. Pertermann, M.; Hirschmann, M.M.; Hametner, K.; Günther, D.; Schmidt, M.W. Experimental determination of trace element partitioning between garnet and silica-rich liquid during anhydrous partial melting of MORB-like eclogite. *Geochem. Geophys. Geosyst.* **2004**, *5*. [CrossRef]

51. Baker, M.B.; Hirschmann, M.M.; Kogiso, T.; Stolper, E.M. Alkalic magmas generated by partial melting of garnet pyroxenite. *Geology* **2003**, *31*, 481–484.

52. Stracke, A.; Bourdon, B. The importance of melt extraction for tracing mantle heterogeneity. *Geochim. Cosmochim. Acta* **2009**, *73*, 218–238. [CrossRef]

53. Salters, V.J.M.; Stracke, A. Composition of the depleted mantle. *Geochem. Geophys. Geosyst.* **2004**, *5*, Q05B07. [CrossRef]

54. Hirose, K. Partial melt compositions of carbonated peridotite at 3 GPa and role of CO_2 in alkali-basalt magma generation. *Geophys. Res. Lett.* **1997**, *22*, 2837–2840. [CrossRef]

55. Hoernle, K.; Tilton, G.; Bas, M.J.L.; Duggen, S.; Garbe-Sch Nberg, D. Geochemistry of oceanic carbonatites compared with continental carbonatites: Mantle recycling of oceanic crustal carbonate. *Contrib. Mineral. Petrol.* **2002**, *142*, 520–542. [CrossRef]

56. Li, S.Z.; Suo, Y.H.; Li, X.Y.; Wang, Y.M.; Cao, X.Z.; Wang, P.C.; Guo, L.L.; Yu, S.Y.; Lan, H.Y.; Li, S.J.; et al. Mesozoic plate subduction in West Pacific and tectono-magmatic response in the East Asian ocean-continent connection zone. *Chin. Sci. Bull.* **2018**, *63*, 1550–1593. (In Chinese) [CrossRef]

57. Huang, J.; Zhao, D. High-resolution mantle tomography of China and surrounding regions. *J. Geophys. Res. Solid Earth* **2006**, *111*. [CrossRef]

58. Kelley, K.A.; Plank, T.; Farr, L.; Ludden, J.; Staudigel, H. Subduction cycling of U, Th, and Pb. *Earth Planet. Sci. Lett.* **2005**, *234*, 369–383. [CrossRef]

59. Hammouda, T. High-pressure melting of carbonated eclogite and experimental constraints on carbon recycling and storage in the mantle. *Earth Planet. Sci. Lett.* **2003**, *214*, 357–368. [CrossRef]

60. Xia, Q.K.; Liu, J.; Kovács, I.; Hao, Y.T.; Li, P.; Yang, X.Z.; Chen, H.; Sheng, Y.M. Water in the upper mantle and deep crust of eastern China: Concentration, distribution and implications. *Natl. Sci. Rev.* **2017**, *6*, 125–144. [CrossRef]

61. Gu, X.Y.; Wang, P.Y.; Kuritani, T.; Hanski, E.; Xia, Q.K.; Wang, Q.Y. Low water content in the mantle source of the Hainan plume as a factor inhibiting the formation of a large igneous province. *Earth Planet. Sci. Lett.* **2019**, *515*, 221–230. [CrossRef]

62. Liu, S.C.; Xia, Q.K.; Choi, S.H.; Deloule, E.; Li, P.; Liu, J. Continuous supply of recycled Pacific oceanic materials in the source of Cenozoic basalts in SE China: The Zhejiang case. *Contrib. Mineral. Petrol.* **2016**, *171*, 1–31. [CrossRef]

63. Vermeesch, P. Tectonic discrimination diagrams revisited. *Geochem. Geophys Geosyst.* **2006**, *7*. [CrossRef]

64. Wang, Y.L.; Zhang, C.J.; Xiu, S.Z. Th/Hf-Ta/Hf identification of tectonic setting of basalts. *Acta Petrol. Sin.* **2001**, *17*, 413–421. (In Chinese)